



Imidazole derivatives as antiparasitic agents and use of molecular modeling to investigate the structure–activity relationship

Oluyomi Stephen Adeyemi^{1,2} · Abiodun Omokehinde Eseola^{3,4} · Winfried Plass³ · Olubunmi Atolani⁵ · Tatsuki Sugi⁶ · Yongmei Han^{6,7} · Gaber El-saber Batiha^{6,8} · Kentaro Kato^{6,9} · Oluwakemi Josephine Awakan¹⁰ · Tomilola Debby Olaolu¹⁰ · Charles Obiora Nwonuma¹⁰ · Omokolade Alejolowo¹⁰ · Akinyomade Owolabi¹¹ · Damilare Rotimi¹⁰ · Omowumi Titilola Kayode¹⁰

Received: 4 September 2019 / Accepted: 15 March 2020
© Springer-Verlag GmbH Germany, part of Springer Nature 2020

Abstract

Toxoplasmosis is a common parasitic disease caused by *Toxoplasma gondii*. Limitations of available treatments motivate the search for better therapies for toxoplasmosis. In this study, we synthesized a series of new imidazole derivatives: bis-imidazoles (compounds 1–8), phenyl-substituted 1*H*-imidazoles (compounds 9–19), and thiopene-imidazoles (compounds 20–26). All these compounds were assessed for in vitro potential to restrict the growth of *T. gondii*. To explore the structure–activity relationships, molecular analyses and bioactivity prediction studies were performed using a standard molecular model. The in vitro results, in combination with the predictive model, revealed that the imidazole derivatives have excellent selectivity activity against *T. gondii* versus the host cells. Of the 26 compounds screened, five imidazole derivatives (compounds 10, 11, 18, 20, and 21) shared a specific structural moiety and exhibited significantly high selectivity (> 1176 to > 27,666) towards the parasite versus the host cells. These imidazole derivatives are potential candidates for further studies. We show evidence that supports the antiparasitic action of the imidazole derivatives. The findings are promising in that they reinforce the prospects of imidazole derivatives as alternative and effective antiparasitic therapy as well as providing evidence for a probable biological mechanism.

Keywords Drug discovery · Infectious diseases · Medicinal biochemistry · Medicinal chemistry

Section Editor: Xing-Quan Zhu

✉ Oluyomi Stephen Adeyemi
oluyomi.stephen.adeyemi@tdtu.edu.vn

¹ Laboratory of Theoretical and Computational Biophysics, Ton Duc Thang University, Ho Chi Minh City, Vietnam

² Faculty of Applied Sciences, Ton Duc Thang University, Ho Chi Minh City, Vietnam

³ Institute of Inorganic and Analytical Chemistry, Friedrich-Schiller-Universität Jena, Humboldtstraße 8, 07743 Jena, Germany

⁴ Department of Chemical Sciences, Redeemer's University, Ede, Nigeria

⁵ Department of Chemistry, University of Ilorin, PMB 1515, Ilorin, Nigeria

⁶ National Research Center for Protozoan Diseases, Obihiro University of Agriculture and Veterinary Medicine, Inada-cho, Obihiro, Hokkaido 080-8555, Japan

⁷ Inner Mongolia University for the Nationalities College of Animal Science and Technology, Tongliao, Inner Mongolia, China

⁸ Department of Pharmacology and Therapeutics Department, Faculty of Veterinary Medicine, Damanhour University, Damanhour, Egypt

⁹ Laboratory of Sustainable Animal Environment, Graduate School of Agricultural Science, Tohoku University, 232-3 Yomogida, Naruko-onsen, Osaki, Miyagi 989-6711, Japan

¹⁰ Department of Biochemistry, Medicinal Biochemistry, Nanomedicine & Toxicology Laboratory, Landmark University, PMB 1001, Omu-Aran 251101, Nigeria

¹¹ Department of Microbiology, Landmark University, PMB 1001, Omu-Aran 251101, Nigeria

Introduction

Toxoplasmosis, which is caused by an intracellular parasite *Toxoplasma gondii*, an apicomplexan (Kamau et al. 2012), is a common parasitic infection in nearly one third of the human population. The life cycle of *T. gondii* is complex in that it exists in three forms, sporozoite, bradyzoite, and tachyzoite. Due to its low host specificity, *T. gondii* can infect a vast array of hosts including animals and humans (Alday and Doggett 2017). The host becomes infected, usually through consumption of either tissue cysts (bradyzoites) in undercooked meat or oocysts (sporozoites) in feline fecal matter. *T. gondii* infections are usually asymptomatic in healthy individuals but can lead to fatal outcomes in immune-compromised individuals (Kamau et al. 2012).

Currently, antimalarial drugs or antibiotics are the treatment of choice for toxoplasmosis. However, the available therapies are fraught with shortcomings such as limited efficacy and poor tolerance (Kamau et al. 2012). According to some reports, the side effects of toxoplasmosis medication caused cessation of treatment in up to 40% of patients (Alday and Doggett 2017; Harrell and Carvounis 2014). Furthermore, although the available therapies for toxoplasmosis are effective against active infections, they do not eradicate latent ones, and relapse is common in patients on suppressive therapy (Alday and Doggett 2017; Harrell and Carvounis 2014). Consequently, toxoplasmosis presents a growing global health burden (Flegr et al. 2014), which is further reinforced by the therapeutic shortcomings highlighted above. Therefore, effective therapeutic agents for toxoplasmosis are urgently required.

Investigations have revealed that screening a vast array of natural or synthetic compounds for potential bioactivity can be an effective approach to the discovery of effective therapies for parasitic diseases (Adeyemi et al. 2017a, b, c, 2018a, b, c, 2019; Castro et al. 2006; Finlayson et al. 2004; Fonseca-Berzal et al. 2014; Grellier et al. 1999). Imidazoles have been reported to possess antiparasitic properties (Coura and Castro 2002; Flores-Holguín and Glossman-Mitnik 2005). Additional investigations have reported both antiparasitic and antimicrobial activity for imidazole-based compounds (Adeyemi et al. 2017a; Liesen et al. 2010). Moreover, imidazole rings are part of many natural compounds including alkaloids, purine, histidine, histamine, and nucleic acids, among others. Furthermore, imidazole rings are part of the chemical structure of antibiotics such as megalzol (2-amino-5-(1-methyl-5-nitro-2-imidazolyl)-1,3,4-thiadiazole), which was first reported as an antimicrobial and later as an excellent trypanocide (Eseola et al. 2011). Other commercially available therapeutic agents that are imidazole derivatives include the antiprotozoan compounds metronidazole and benzimidazole and the antifungal compounds

asmiconazole and ketoconazole. In light of these facts, we synthesized a new series of imidazole derivatives that could be grouped into *bis*-imidazoles, phenyl-substituted *1H*-imidazoles, and thiopene-imidazoles. All compounds were screened for in vitro potential to restrict the growth of *T. gondii* as well as by in silico modeling for bioactivity.

Materials and methods

General

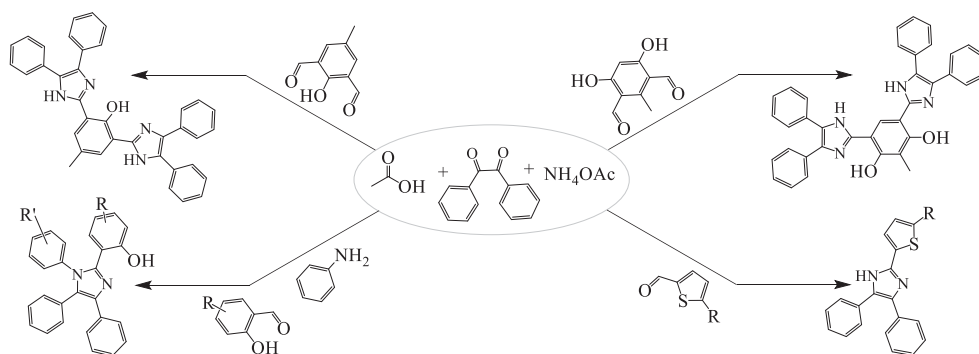
Materials, reagents, and substrates for the experimental syntheses and catalysis were commercially sourced as reagent grade and used as supplied. The synthesis and characterization of compounds C-1–C-8, and C-16–C-26 followed established methodologies (Eseola et al. 2012, 2018, 2019; Lipinski et al. 1997). Impurities were removed from the imidazole-based compounds by either recrystallization or silica gel column chromatography. Elemental analyzers (Leco CHNS-932 or vario EL Cube) were used to determine the elemental composition, while a Bruker 400 MHz instrument was used to obtain ^1H and ^{13}C NMR spectra, using deuterated solvents as the internal standard. A Bruker Equinox spectrophotometer equipped with diamond ATR in the range of 4000–370 cm^{-1} was used to obtain the IR spectra. The general synthesis of the imidazole derivatives is shown in Scheme 1, while further synthetic protocols are presented below.

Synthetic protocols

Compound 9—2-(1,4,5-triphenyl-1H-imidazol-2-yl)phenol

1.2 g of salicylaldehyde, 2.0 g of benzil, 1.3 g of aniline, and 2.2 g of ammonium acetate were refluxed in glacial acetic acid. After a 3-h reflux, a whitish crystalline product was formed in the flask, which was immediately filtered and washed with water, and the product was dried at 40 °C to obtain compound C-9. (3.3 g, 89%). Mp. 258 °C. Selected IR peaks (ATR): ν 3063 m (C–H aromatic), 1588s (C=C or C=N), 1482vs, 749vs, 692vs. ^{13}C NMR (101 MHz, *d6*-DMSO) δ 149.36, 149.14, 148.90, 148.11, 145.11, 134.32, 133.64, 131.81, 131.49, 130.28, 129.55, 129.17, 128.92, 127.37, 126.50, 121.21, 118.78, 118.11, 114.22, 113.16, 113.05, 111.68, 56.25, 56.22, 55.93. ^{13}C NMR (101 MHz, *d6*-DMSO) δ 157.76, 144.90, 137.03, 134.83, 133.64, 131.74, 131.22, 130.66, 130.09, 129.85, 129.73, 129.19, 129.12, 128.98, 128.92, 127.39, 127.26, 126.57, 118.59, 117.40, 114.32. MS: 388 (100.0%), 388, 267, 194, 165, 77.

Scheme 1 Representative scheme for the synthesis of imidazole derivatives



Compound 10—1-(1,4,5-triphenyl-1H-imidazol-2-yl)naphthalen-2-ol

Benzil (1.20 g, 5.75 mmol), 2-hydroxynaphthalene-1-carbaldehyde (0.99 g, 5.75 mmol), aniline (0.64 g–0.64 mL, 0.69 mmol), and ammonium acetate (1.33 g, 17.25 mmol) were treated as in the preparation of C-9, but the purification was carried out on a silica gel column using 100% chloroform to remove impurities followed by washing with 100% ethyl acetate to elute compound C-10 as colorless crystalline blocks (1.34 g, yield = 53%). Mp. 269 °C. Selected IR peaks (ATR): ν 3051 m, 1618 m, 1595s, 1493s, 690vs, 518s. ^1H NMR (400 MHz, CDCl_3) δ 7.59 (t, $J=6.6$ Hz, 3H), 7.45 (t, $J=8.5$ Hz, 2H), 7.33–7.25 (m, 4H), 7.23–7.13 (m, 4H), 6.95 (q, $J=6.9$ Hz, 5H), 6.88 (d, $J=6.7$ Hz, 2H), 6.73 (d, $J=8.8$ Hz, 1H). ^{13}C NMR (101 MHz, CDCl_3): δ 155.14, 143.93, 136.88, 136.08, 133.71, 132.49, 131.18, 130.17, 130.10, 128.33, 128.21, 128.14, 127.75, 127.53, 127.28, 127.23, 126.82, 126.08, 124.22, 122.85, 119.39, 109.91. MS (EI) m/z 438 (M^+ , 100%): 438, 421, 361, 267. Anal. Calc. for $\text{C}_{31}\text{H}_{22}\text{N}_2\text{O}$: C, 84.91; H, 5.06; N, 6.39%. Found: C, 84.62; H, 5.08; N, 6.40%.

Compound 11—4-methoxy-2-(1,4,5-triphenyl-1H-imidazol-2-yl)phenol

Benzil (1.0 g, 4.8 mmol), 2-hydroxy-5-methoxybenzaldehyde (0.7 g, 4.8 mmol), aniline (0.4 g, 4.8 mmol), ammonium acetate (1.1 g, 14.3 mmol), and 15 mL of glacial acetic acid were reacted as for C-9 above. The resulting precipitate, compound C-11, was filtered and purified by column chromatography (1.1 g, yield = 49%). MP = 217 °C. Selected IR peaks (KBR): ν 3430, 3057, 1595, 1224. ^1H NMR (400 MHz, d_6 -DMSO) δ 12.29 (s, 1H), 7.44 (d, $J=6.3$ Hz, 7H), 7.34–7.27 (m, 7H), 7.38–7.25 (m, 7H), 7.23 (t, $J=7.3$ Hz, 1H), 6.89 (d, $J=8.9$ Hz, 1H), 6.79 (dd, $J=8.9, 3.0$ Hz, 1H), 6.20 (d, $J=3.0$ Hz, 1H), 3.26 (s, 3H). ^{13}C NMR (101 MHz, d_6 -DMSO) δ 151.82, 151.23, 144.65, 137.09, 134.78, 133.53, 131.77, 131.34, 130.01, 129.98, 129.84, 129.33, 129.25, 129.00,

128.94, 127.45, 126.55, 118.14, 117.34, 113.63, 111.04, 55.15. MS (EI) m/z 418 (M^+ , 100%): 418, 403 (–methyl), 209, 165, 77.

Compound 12—4-tert-butyl-2-(1-(4-methoxyphenyl)-4,5-diphenyl-1H-imidazol-2-yl)phenol

Benzil (1.0 g, 4.8 mmol), 5-tert-butyl-2-hydroxybenzaldehyde (0.9 g, 4.8 mmol), *p*-methoxyaniline (0.6 g, 4.8 mmol), ammonium acetate (1.1 g, 14.3 mmol), and 15 mL of glacial acetic acid were reacted as for compound 9 to obtain compound C-12 (1.2 g, 52%). MP = 209 °C. Selected IR peaks (KBR): ν 3450, 3024, 1606, 1250. ^1H NMR (400 MHz, d_6 -DMSO) δ 12.87 (s, 1H), 7.43 (d, $J=7.2$ Hz, 2H), 7.39–7.27 (m, 9H), 7.25–7.18 (m, 2H), 7.00–6.97 (m, 2H), 6.90 (d, $J=8.6$ Hz, 1H), 6.75 (d, $J=2.4$ Hz, 1H), 3.74 (s, 3H), 0.93 (s, 9H). ^{13}C NMR (101 MHz, d_6 -DMSO) δ 160.06, 155.71, 145.29, 140.39, 134.32, 133.53, 131.82, 131.49, 130.48, 130.12, 129.87, 129.22, 129.00, 128.94, 127.41, 126.49, 123.54, 116.94, 115.27, 112.75, 55.97, 33.88, 31.29. MS (EI) m/z 474 (M^+ , 100%): 474, 459, 237, 165, 77.

Compound 13—2-(1-(4-methoxyphenyl)-4,5-diphenyl-1H-imidazol-2-yl)phenol

Benzil (2.0 g, 9.5 mmol), salicylaldehyde (1.4 g, 9.5 mmol), *p*-methoxyaniline (1.2 g, 9.5 mmol), ammonium acetate (2.2 g, 28.6 mmol), and 15 mL of glacial acetic acid were reacted as for compound 9 and purified by a 1:2:20 mixture of ethyl acetate/dichloromethane/*n*-hexane over a silica gel column to obtain compound C-13 (1.4 g, 34%). MP = 206 °C. Selected IR peaks (KBR): ν 3061 m (C–H aromatic), 2843 m (methyl), 1604s (C=C or C=N), 1583s (C=C or C=N), 1512vs, 1247vs, 696vs. ^1H NMR (400 MHz, d_6 -DMSO) δ 12.84 (s, 1H), 7.44 (d, $J=7.3$ Hz, 2H), 7.35–7.26 (m, 9H), 7.23 (d, $J=7.2$ Hz, 1H), 7.17 (dd, $J=11.4, 4.5$ Hz, 1H), 6.97 (d, $J=7.8$ Hz, 1H), 6.92 (d, $J=8.9$ Hz, 2H), 6.71 (dd, $J=8.0, 1.4$ Hz,

1H), 6.57 (dd, $J=11.2, 4.0$ Hz, 1H), 3.74 (s, 1H). ^{13}C NMR (101 MHz, *d6*-DMSO) δ 159.77, 157.92, 145.10, 134.57, 133.65, 131.77, 131.56, 130.57, 130.30, 130.19, 129.59, 129.17, 128.98, 128.91, 127.36, 126.93, 126.54, 118.62, 117.49, 114.93, 114.19, 55.79. MS (EI) m/z 418 (M^+ , 100%): 418, 403 (–methyl), 373, 209, 165, 77.

Compound 14—2-methoxy-6-(1-(3,4-dimethoxyphenyl)-4,5-diphenyl-1H-imidazol-2-yl)phenol

Benzil (2.0 g, 9.5 mmol), 2-hydroxy-3-methoxybenzaldehyde (1.5 g, 9.5 mmol), 3,4-dimethoxybenzenamine (1.6 g, 9.5 mmol), and ammonium acetate (2.2 g, 28.6 mmol) in glacial acetic acid were reacted as for compound C-9 and purified by 2:5 of ethyl acetate/*n*-hexane over a silica gel column to obtain compound C-14 (3.57 g, 78%). MP = 203 °C. Selected IR peaks (KBR): ν 3064 m (C–H aromatic), 3011 m (C–H aromatic), 2939 m (methyl), 2831 m (methyl), 1591s (C=C or C=N), 1512vs, 1244vs, 777vs. ^1H NMR (400 MHz, *d6*-DMSO) δ 12.86 (s, 1H), 7.47–7.42 (m, 2H), 7.35–7.27 (m, 7H), 7.22 (t, $J=7.3$ Hz, 1H), 7.06 (d, $J=2.2$ Hz, 1H), 6.95–6.85 (m, 3H), 6.55 (t, $J=8.1$ Hz, 1H), 6.37 (dd, $J=8.2, 1.2$ Hz, 1H), 3.80 (s, 3H), 3.74 (s, 3H), 3.60 (s, 3H). ^{13}C NMR (101 MHz, *d6*-DMSO) δ 149.36, 149.14, 148.90, 148.11, 145.11, 134.32, 133.64, 131.81, 131.49, 130.28, 129.55, 129.17, 128.92, 127.37, 126.50, 121.21, 118.78, 118.11, 114.22, 113.16, 113.05, 111.68, 56.25, 56.22, 55.93. MS (EI) m/z 478 (M^+ , 100%): 478, 461, 449, 435, 165.

Compound 15—2-(1-phenyl-1H-phenanthro[9,10-d]imidazol-2-yl)phenol

Phenanthrenequinone (2.1 g, 10.0 mmol), 2-hydroxybenzaldehyde (2.2 g, 10.0 mmol), aniline (3.7 g, 40.0 mmol), and ammonium acetate (3.1 g, 40.0 mmol) in glacial acetic acid were reacted as for compound C-9 and purified by 2:5 of a dichloromethane/*n*-hexane mixture as eluent over a silica gel column to obtain compound C-15 (3.2 g, 83%). MP = 178 °C. Selected IR peaks (KBR): ν 3051 m (C–H aromatic), 1584s (C=C or C=N), 1480vs, 753vs. ^1H NMR (400 MHz, *d6*-DMSO) δ 11.88 (s, 1H), 8.95 (s, 1H), 8.89 (d, $J=8.4$ Hz, 1H), 8.62 (dd, $J=7.9, 0.9$ Hz, 1H), 7.80 (t, $J=7.3$ Hz, 1H), 7.75–7.67 (m, 6H), 7.59–7.54 (m, 1H), 7.34 (t, $J=7.4$ Hz, 1H), 7.27–7.20 (m, 1H), 7.06–7.00 (m, 2H), 6.98–6.92 (m, 1H), 6.70–6.61 (m, 1H). ^{13}C NMR (101 MHz, *d6*-DMSO) δ 157.86, 149.43, 138.53, 135.23, 131.41, 130.84, 130.81, 129.25, 129.17, 129.02, 128.18, 128.13, 127.29, 127.20, 126.42, 126.35, 125.87, 125.01, 124.23, 122.68, 122.31, 120.73, 118.71, 117.15, 115.65. MS (EI) m/z 386 (M^+ , 100%): 386, 369, 266, 193, 178, 77.

Parasite

In this study, the *T. gondii* RH strain 2F (ATCC® 50839) was used. To maintain the parasite, *T. gondii* was repeatedly passaged in cultures of human foreskin fibroblast (HFF; ATCC®) cells in a medium composed of Dulbecco's modified Eagle's medium (DMEM; Nissui, Tokyo, Japan), 1% L-glutamine (200 mM; Gibco, Fisher Scientific, UK), 10% (v/v) fetal bovine serum (FBS; Gibco, Fisher Scientific, UK), and penicillin and streptomycin (100 U/mL; Biowhittaker, UK). To purify the parasite for the antiparasite assays, *T. gondii*-infected HFF cells were lysed, filtered, and washed three times in fresh medium.

In vitro assays for inhibition of parasite growth

Imidazole derivatives were prepared in dimethyl sulfoxide (DMSO, Sigma-Aldrich), to make stock solutions that were screened for antiparasitic action at various concentrations between 0.01 and 10 μM .

The in vitro assays for inhibition of parasite invasion and growth were performed as described previously (Adeyemi et al. 2017b). In brief, the test compounds in the cell culture medium (as highlighted above) were added to newly purified parasites in growing HFF cells, while the medium lacking the test compounds served as the negative drug control. After a 72-h incubation in an atmosphere of 37 °C and 5% CO_2 , parasite viability was determined by assaying for galactosidase activity using a Promega Beta-Glo reagent kit (Madison, USA) and following the manufacturer's instructions. The luminescence signal was acquired on a Multi Detection System plate reader (GloMax® Promega Japan). The final concentration of DMSO in the cultures was <0.1% (v/v). To validate the assay, pyrimethamine was included as reference drug(s). The biological evaluation was in triplicate and independently replicated thrice. The Nunc 96-well optical bottom plate (Fisher Scientific, Pittsburgh, USA) was used for the assay unless otherwise indicated.

The cytotoxic potential of imidazole derivatives

The HFF cells were cultured in DMEM as indicated above. At confluence, the cells were sub-cultured into 96-well plates at a concentration of 1×10^5 cells per well. After a 72-h incubation at 37 °C and 5% CO_2 , the imidazole compounds (between 0.01 and 10 μM) in the cell culture medium were added, while the culture medium lacking imidazole derivatives served as the negative drug control. To validate the assay, staurosporine (1 μM , final concentration) was used as a positive control drug. After a 72-h incubation, the colorimetric determination of cell viability (Promega CellTitre-Aqueous One kit; Madison,

USA) was at 490 nm on a microplate reader (MTP 500; Corona Electric, Hitachinaka, Japan). The biological evaluation was carried out in triplicate and independently replicated thrice.

Immunofluorescence assays (IFA)

Invasion

The invasion assays were carried out as reported elsewhere (Adeyemi et al. 2017b). In brief, purified parasites [1×10^5] with the various imidazole-based compounds (at double IC_{50} for each compound) in a culture medium were added to HFF monolayers growing on a coverslip. The medium only served as negative drug control. After a 1-h incubation at 37 °C, the cells were washed and stained on ice with polyclonal rabbit anti-*T. gondii* antibodies [1:1000] (Bio-Rad Laboratories, USA) in washing buffer (2% FCS-PBS) for 30 min. Thereafter, the cells were fixed with 4% paraformaldehyde in PBS and permeabilized with ice-cold methanol. Then, the cells were primarily stained with anti-SAG1 antibodies [1:1000] (Hyttest, Finland), while Alexa Fluor 488 anti-mouse antibody, Alexa Fluor 594 anti-rabbit antibody, and DAPI [1:1000] were used for secondary staining. Visualization of the stained cells was performed on a fluorescence microscope (Nikon Eclipse E400, Tokyo, Japan), with at least 50 microscopic fields randomly selected. Rabbit anti-*T. gondii* antibodies were used to detect the extracellular parasites, while anti-SAG1 antibodies were used to detect the total parasites.

Intracellular doubling

Intracellular doubling assays were carried out as previously reported (Adeyemi et al. 2017b). In brief, purified parasites (1×10^5) were added to HFF monolayers growing on a coverslip. After a 1-h incubation at 37 °C, the cells were washed three times with culture medium to remove non-invaded parasites. Fresh culture containing imidazole-based compounds was added while medium lacking imidazoles served as the negative drug control. After 24-h incubation at 37 °C, the cells were fixed with 4% paraformaldehyde in PBS and permeabilized with ice-cold methanol. Thereafter, a blocking buffer (2% BSA in 0.1% Tween 20-PBS) was added to the cells and after 1-h incubation at room temperature, the primary staining was done with anti-SAG1 antibodies (1:1000) (Hyttest, Finland) in a blocking buffer, while the Alexa Fluor 594 goat anti-mouse antibody and DAPI were used for secondary staining. The stained cells were viewed on a fluorescence microscope (Nikon Eclipse E400, Tokyo, Japan). To count the parasitophorous vacuoles and estimate the number of tachyzoites per vacuole, at least 50 microscopic fields were randomly viewed.

Molecular modeling studies: descriptors and potential bioactivities evaluation

To explore the antiparasitic potential of the synthesized compounds, molecular modeling was used to evaluate the physicochemical characteristics (structural profile) and potential bioactivities (enzyme inhibition) using on-line chemoinformatics tools (<http://www.molinspiration.com>). The compounds were optimized on the Chemdraw software (Lipinski et al. 2001) and the simplified molecular-input line-entry system (SMILES) format fed into the Molinspiration program. The structural profile of compounds such as the partition coefficient (octanol/water), total polar surface area, molecular weight, molecular volume, the number of hydrogen bond acceptors/donors, number of rotatable bonds, and degree of violation of Lipinski's rule (Lipinski 2004; Atolani et al. 2014) for drug-likeness were evaluated following reported standard procedures (Rocha-Roa et al. 2018; Flores-Holguín and Glossman-Mitnik 2004). Likewise, the bioactivity score based on ion channel modulation, potential as GPCR ligand, kinase inhibition, nuclear receptor interaction, protease inhibition, and enzyme inhibition were also calculated to give insight into the biological potential of the compounds (Lipinski 2004; Atolani et al. 2014). The bioactivity measurement is premised on Lipinski's "rule of five," which evaluates the similarity of the molecular properties and structural features of a molecule to those of known drugs.

Ranking of compounds based on toxicological risks

Furthermore, the imidazole compounds were ranked based on toxicological risks prediction using PROTOX II modeling (http://tox.charite.de/protox_II/index.php?site=compound_input). The PROTOX II allows for sorting or ranking according to possible toxicological risks, by comparing input compounds with dataset compounds using the SMILES codes.

Statistical analysis

A one-way ANOVA (GraphPad, San Diego, CA, USA) was used to analyze the results. The data are presented as the mean \pm standard error of mean (SEM). The Dunnett post hoc test was used to compare the groups, and the mean values were significant at $p < .05$. The concentration that caused inhibition of *T. gondii* growth or cellular toxicity by 50% (EC_{50} and/or IC_{50}) was estimated from a dose-response curve of the compound concentrations versus the viability of either the parasite or the host cell. The curve was fitted using a non-linear regression analysis.

Results and discussion

Chemistry of imidazole derivatives

Scheme 1 shows the synthetic routes for the imidazole compounds depicted in Scheme 2. Theazole derivatives were designed to allow for modifications based on electronic and steric considerations. Within the *bis*-imidazoles, phenyl-substituted *1H*-imidazoles, or thiophene-imidazoles, the electronic differential was designed to allow for electron-releasing or electron-withdrawing exchanges. Thus, the intermolecular interaction potential of compounds is likely to differ considerably.

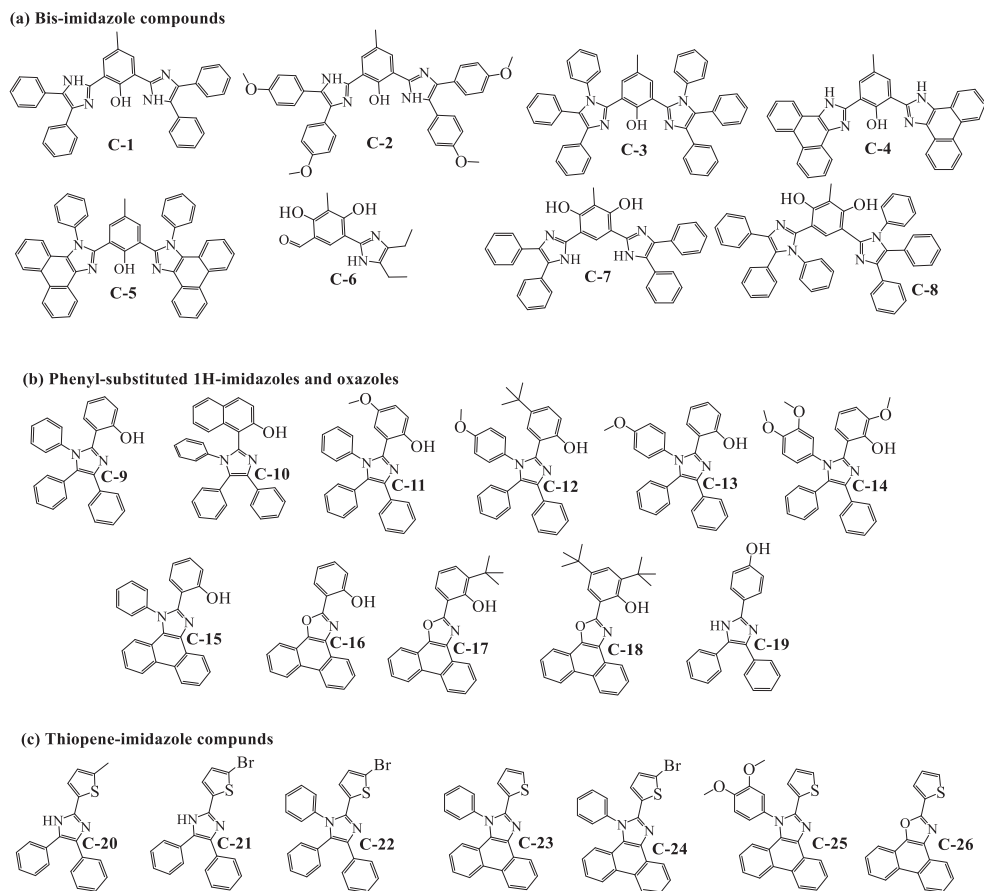
The identities of the synthesized molecules were established using mass spectrometry and/or elemental analysis in addition to spectroscopic data (NMR and FTIR). X-ray structural confirmations were also obtained for representative members of each molecular group, as presented in Fig. 1. Based on previous studies (Eseola et al. 2012, 2018, 2019), it is important to mention that molecules bearing unsubstituted imidazole protons possess notably different electronic characteristics compared with their analogues that have phenyl or alkyl

substituents. Furthermore, strong intra- and intermolecular interactions are often observed for theseazole molecules via hydrogen bonding and π - π stacking interactions, as was displayed by the dimeric pairing in the structure of compound C-10 (Eseola et al. 2019).

Biological assays

The *in vitro* screening of synthetic or natural compounds is hinged on the fact that the screening of a vast array of compounds may allow for the identification of likely lead candidates for neglected tropical diseases (Adeyemi et al. 2017a, b, c, 2018a, b, c, 2019). In this study, we synthesized a new series of imidazole derivatives and evaluated these compounds (Scheme 2) for anti-*T. gondii* properties. The synthesis of the new series of imidazole derivatives followed our recent report (Adeyemi et al. 2017a), which showed that compounds containing an imidazole ring are promising antiprotozoal agents. In the current study, the antiparasite assays revealed that the imidazole derivatives strongly restricted the growth of *T. gondii* (Fig. 2), with the EC_{50} ranging between 0.003 and 16 μ M (Table 1). Meanwhile, the estimated selectivity index showed

Scheme 2 Imidazole compounds according to structural grouping: (a) *bis*-imidazoles, (b) imidazole-phenols, and (c) thiophene-azoles



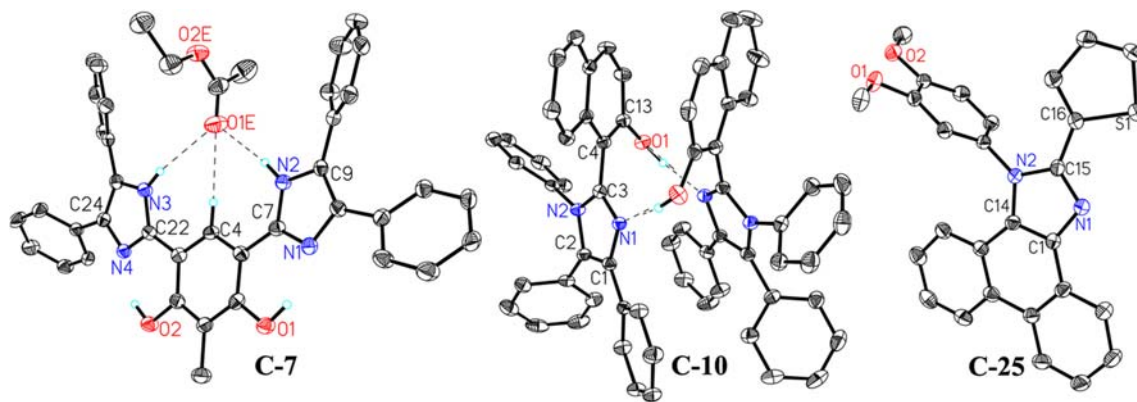


Fig. 1 Ortep structural plot for probe molecules C-7 (left), C-10 (middle), and C-25 (right). Some hydrogen atoms and co-crystallized solvent molecules have been omitted for clarity

appreciable selective action (< 1- to > 27,666-fold activity) towards the parasite versus the host cell, suggesting specific antiparasitic potential by the imidazole derivatives. The imidazole derivatives significantly suppressed the parasite growth with an average of $\geq 75\%$, $\geq 90\%$, and $\geq 91\%$ for *bis*-imidazoles, phenyl-substituted *1H*-imidazoles, and thiopene-imidazoles, respectively (Table 2). These antiparasitic activities by imidazole compounds not only compared favorably with that of the reference drug, pyrimethamine but also showed no apparent toxicity to the host cells, even up to the highest concentration, 10 μM , used in this study. While most of the imidazole compounds showed good selective action against the parasite versus the host cells, phenyl-substituted *1H*-imidazoles (C-10, C-11, C-12, C-14, and C-18) and thiopene-imidazoles (C-20 and C-21) showed the most specific action against the parasite. Taken together, our current findings are consistent with studies that demonstrated that compounds containing an imidazole ring possess antiprotozoal properties (Coura and Castro 2002; Flores-Holguín and Glossman-Mitnik 2005; Liesen et al. 2010). In addition, Liesen, et al. (Berkelhammer and Asato 1969) reported that a series of thiadiazole derivatives showed promising anti-*T. gondii* activity when compared with a standard drug, sulfadiazine. The findings indicate that compounds containing imidazole rings are a potential source of alternative antiparasitic agents. Furthermore, reports have shown that imidazole-based compounds are active against *T. gondii* likewise as other compounds based on similar chemical scaffold (Dzitko et al. 2014; Tessmann et al. 2017).

Moreover, several currently available therapeutic agents, such as metronidazole, benznidazole, mefloquine, miconazole, and ketoconazole, contain imidazole rings.

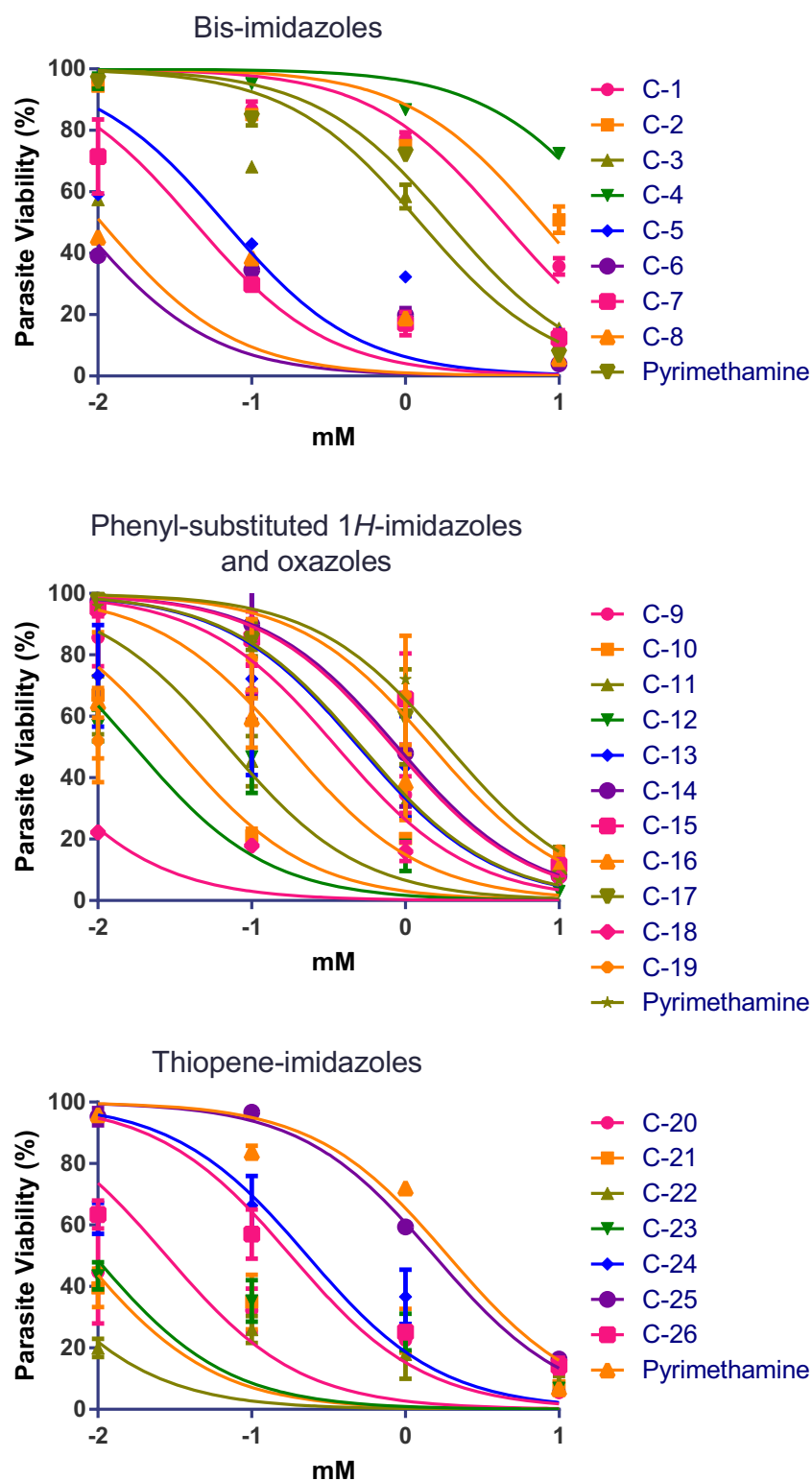
For further experiments, only imidazole compounds with greater selectivity index ≥ 100 were selected. These include

C-7, C-10, C-11, C-12, C-14, C-18, C-20, and C-21. The SI was estimated as the ratio of the host toxicity (EC_{50}) to parasite toxicity (IC_{50}).

Imidazole derivatives affect the invasion and intracellular replication cycle in *T. gondii*

To preliminarily establish the mechanistic antiparasitic action of the imidazole derivatives, we determined whether the *T. gondii* lytic cycle was affected. The lytic cycle of *T. gondii* is a repeated process of invasion, replication, and egress. Therefore, we used IFA to determine whether the imidazole derivatives affected the invasion and intracellular doubling of the parasite. The data revealed a dramatic decrease in the capacity of the parasite to invade monolayers of HFF cells by 80 to 40% (Fig. 3a). Similarly, the imidazole derivatives appreciably decreased the number of parasites per vacuole (Fig. 3b), resulting in a > 70% reduction in average parasitic replication per vacuole (> 100 vacuoles counted per experiment) compared with the control (Fig. 3c). Furthermore, imidazole derivatives depleted the number of parasites per vacuole (Fig. 3d); < 8 parasites per vacuole for the imidazole derivatives compared with the negative drug control, in which the parasites per vacuole increased steadily. Representative fluorescent images of the IF staining are presented in Figs. 4 and 5. Taken together, our findings established that the imidazole derivatives significantly influenced the invasion and replication processes of the *T. gondii* lytic cycle, thus yielding an early perspective about how imidazole derivatives restrict parasite growth. Additionally, the depleted parasite vacuoles and parasites per vacuole suggest that the imidazole derivatives arrested the replication of *T. gondii* rather than slowed it. Also, it is unlikely that the depletion in parasite vacuoles was a result of the parasite egressing prematurely from the host

Fig. 2 Dose–response curve after a 72-h treatment with imidazoles. Data are expressed as the mean \pm standard error of mean (SEM)



cells; the host cells were apparently intact and extracellular parasites were not observed. Taken together, the data indicate that imidazole derivatives may be clearing the parasites through an as yet unknown host-mediated mechanism.

Structure–activity relationships: anti-*T. gondii* activity

Exploring the structure–activity relationship (SAR), the electron-donating or electron-withdrawing substituents on the phenyl moieties as well as the steric bulkiness due to the

Table 1 Estimation of EC₅₀ and selectivity index for imidazole derivatives

Compounds	EC ₅₀ (anti- <i>Toxoplasma gondii</i>) μM	IC ₅₀ (host cells—HFF) μM	Selectivity index (SI)
C-1	4.334	49	11
C-2	7.617	260	34
C-3	1.285	20	15
C-4	14.81	57	3
C-5	1.103	60	54
C-6	0.814	10	12
C-7	0.038	4	105
C-8	0.915	2	2
C-9	0.302	5	16
C-10	0.034	40	1176
C-11	0.123	105	853
C-12	0.014	36	2571
C-13	0.182	0.1	1
C-14	0.377	254	673
C-15	0.753	ND	ND
C-16	0.113	ND	ND
C-17	0.519	ND	ND
C-18	0.003	83	27,666
C-19	0.702	ND	ND
C-20	0.024	85	3541
C-21	0.006	10	1666
C-22	0.003	ND	ND
C-23	0.008	ND	ND
C-24	0.183	20	109
C-25	1.459	72	49
C-26	0.139	2	14
Pyrimethamine	1.906	10	5

The EC₅₀ and/or IC₅₀ were estimated from a dose–response curve of the compound concentrations versus the viability of either the parasite or the host cell respectively. The curve was fitted using a non-linear regression analysis on a GraphPad Prism 5

ND not determined

presence of aromatic rings may play a role in the differential activity towards the parasite as well as towards the host cells. While electronic effects could be considered to play a role in the action of the tested compounds, the electron-donating or electron-withdrawing capacity of the aromatic substituents did not appear to dramatically alter the anti-*T. gondii* activity, although it might have contributed to differential host cell toxicity, thereby giving rise to the low or high selective antiparasitic action. Additionally, the hydrophobic nature of the phenyl rings might have been responsible for differential activity exhibited by the compounds.

The compounds C-1, C-2, C-3, C-4, and C-5 that bore one hydrophobic *o*-CH₃ on their central rings with large cyclic hydrocarbon moieties apparently confer poorly specific anti-*T. gondii* activity on the molecules (Table 1), probably due to the high molecular weights of the compounds. This suspicion

was supported by the results obtained from the molecular description analysis (Table 3). The *bis*-imidazoles apparently had too high a partition coefficient (miLog $P > 5.0$) and molecular weight (> 500), which might have limited their bio-availability and absorption by the parasite membrane. A high log P value is an indication of increased hydrophobicity, which retards the penetration of the compound through the parasite membrane, thereby reducing the concentration of compounds reaching the target action site. The high carbon-to-hydrogen ratio may also have contributed to reducing the antiparasitic activities, but with increased toxicity to the host cells. Increased hydrophobicity has been reported to reduce the bio-activity of other compounds (Lavorato et al. 2017; Rutkowska et al. 2017). The presence of the hydrophilic *o*-OCH₃ groups on C-2 seems not to have enhanced the antiparasitic activity but affected the selectivity by increasing the toxicity to the

Table 2 Parasite inhibition and host cell viability

Compounds	Parasite inhibition (%) ^a	Parasite average inhibition (%)	Host cell viability (%) ^b
C-1	64.30 ± 2.68	74.90	108.84 ± 9.66
C-2	49.12 ± 4.29		109.51 ± 14.06
C-3	84.48 ± 0.65		110.57 ± 7.98
C-4	37.58 ± 0.37		107.76 ± 6.56
C-5	85.73 ± 1.39		106.30 ± 6.48
C-6	96.07 ± 0.64		103.31 ± 2.30
C-7	87.65 ± 2.58		6.30 ± 1.35
C-8	94.29 ± 0.89		122.86 ± 11.93
C-9	92.53 ± 0.58	90.51	97.90 ± 3.39
C-10	87.77 ± 2.59		96.65 ± 2.30
C-11	87.57 ± 5.03		128.40 ± 23.54
C-12	97.01 ± 4.91		102.31 ± 11.85
C-13	91.77 ± 6.49		117.92 ± 17.96
C-14	91.86 ± 7.35		90.71 ± 1.06
C-15	88.52 ± 4.84		137.62 ± 23.01
C-16	89.48 ± 2.27		149.81 ± 16.53
C-17	92.83 ± 5.46		104.41 ± 6.90
C-18	92.60 ± 1.01		146.42 ± 4.26
C-19	83.72 ± 5.48		108.41 ± 13.90
C-20	94.50 ± 3.81	90.71	104.77 ± 3.55
C-21	92.26 ± 7.10		124.90 ± 5.75
C-22	92.02 ± 7.94		121.16 ± 12.88
C-23	93.09 ± 5.96		114.98 ± 7.74
C-24	93.72 ± 8.83		89.02 ± 1.44
C-25	83.59 ± 6.17		110.19 ± 3.33
C-26	85.78 ± 1.06		104.82 ± 10.11

^a Parasite growth inhibition values from screening with RH-2F at 10 μM. DMSO control was calculated as 0% inhibition, and 10 μM pyrimethamine control was calculated as 100% growth inhibition

^b Host cell viability values from preliminary screening with HFF cells at 10 μM concentration. DMSO control was calculated as 100% cell viability

host cells. C-3, an analog of C-1, was found to possess improved selectivity to the parasite owing to the addition of two hydrophobic phenyl groups.

Fused aromatic rings (phenanthrene moieties), which reduced the number of rotatable bonds to 2 (Table 2) and thereby conferred increased rigidity in C-4, seem to have increased host cell toxicity while decreasing selective activity towards the parasite compared with C-1 or C-5. The addition of the phenanthrene moiety might have conferred electron-withdrawing capacity on the *bis*-imidazoles, and this may have enhanced the compounds' reactivity with the cellular membrane or macromolecules. This is consistent with our recent report (Flegr et al. 2014), which found that fusing aromatic rings increased bulkiness and enhanced host cytotoxicity. C-4 and C-5 are structurally the same except for the additional phenyl groups symmetrically attached to two of the four heteroatoms (nitrogen), thereby improving the flexibility of the molecule for interactions with the parasite. The phenolic derivative C-6 had significant anti-*T. gondii* activity although

with low selectivity, apparently as a result of its molecular size and polarity. C-6, a very polar compound, was the compound with the smallest molecular weight, molecular volume, and partition coefficient (Table 3). Small molecules are renowned for having greater biological activity. Moreover, phenolic compounds are well reported as having strong interactions with biological molecules because of their potential to easily form phenoxide ions (Qasim et al. 2017). Therefore, the high carbon-to-hydrogen ratio in C-7 to C-9 may partially account for the selectivity observed. It is no surprise that C-7 had low selectivity in that it is the only compound that violated as many as three of Lipinski's rules (Table 3).

On the other hand, the electron-donating capacity and reduced bulkiness of C-10 and C-11 may have enhanced their selective action against the parasite versus the host cell when compared with the others in the same group (C-12 to C-14). The presence of an alkyl substituent in C-12 could have weakened its electron-donating capacity, thus making it less reactive than C-11 or C-14. These observations were consistent

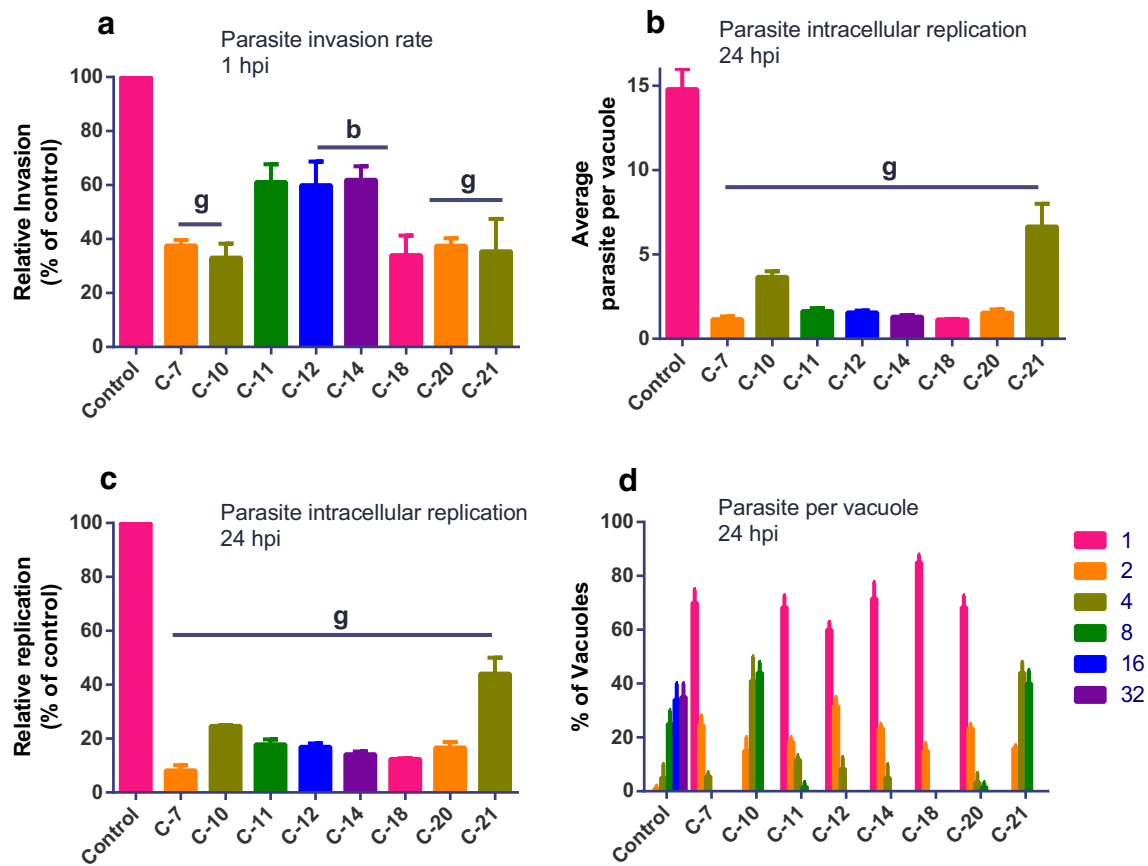


Fig. 3 Immunofluorescence (IF) staining of *T. gondii*-infected HFF cells that were treated with imidazole derivatives. **a** Freshly purified parasite suspension and imidazole derivatives were added to growing HFF monolayers on coverslips. Invasion was allowed for 1 h before IF staining. **b** Average parasites per vacuole following treatment with imidazole derivatives. Freshly purified parasite suspensions were added to growing HFF monolayers on coverslips. Invasion was allowed for 1 h, after which the infection medium was replaced with fresh medium containing imidazole

derivatives. IF staining of intracellular parasites was carried out after 24-h. **c** Percentage replication of intracellular parasite. **d** Parasite numbers based on 100 parasitophorous vacuoles after treatment with imidazole derivatives for 24-h incubation. Data are expressed as the mean \pm standard error of mean (SEM). Experiment was repeated three times independently. β is significant at $p < .001$ while γ is significant at $p < .0001$ relative to the control

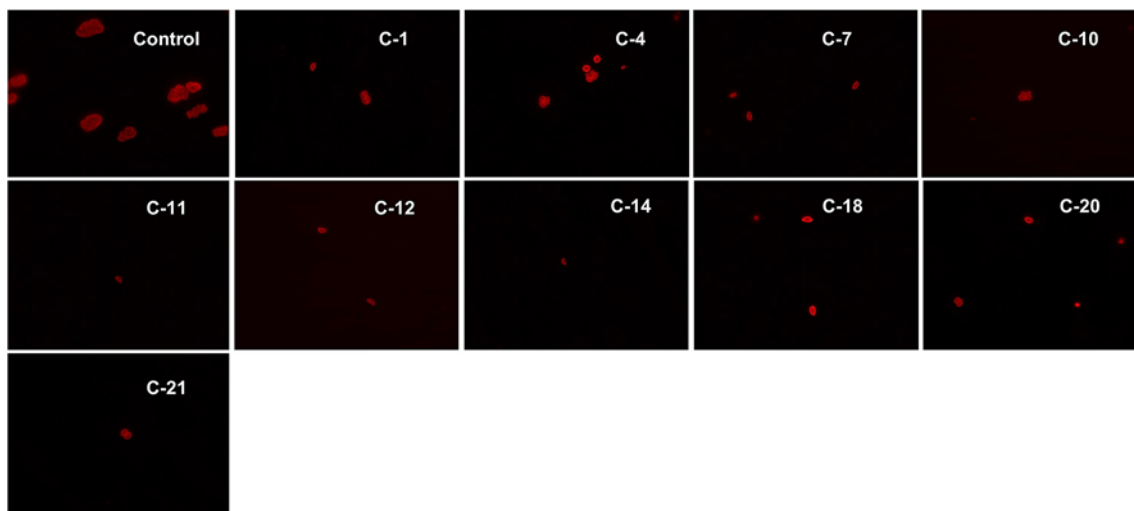


Fig. 4 Representative fluorescent images showing replicating tachyzoites (RH-2F strain) only at 24-h incubation with either culture medium only (control) or imidazole derivatives

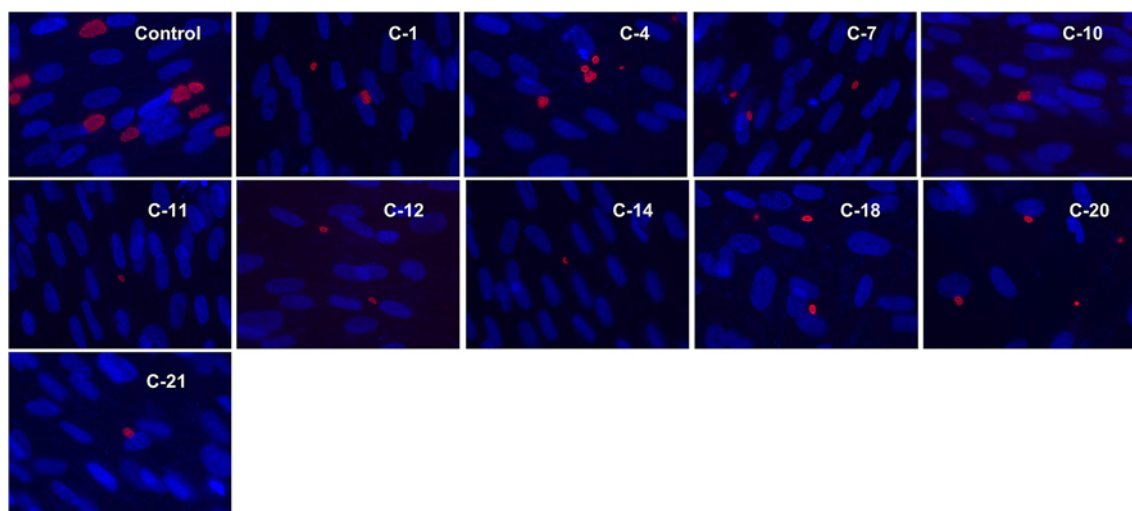


Fig. 5 Representative fluorescent images showing replicating tachyzoites (RH-2F strain) with nuclear staining (DAPI) at 24-h incubation. IF staining was performed following treatment with imidazole derivatives. Each experiment was performed three times independently.

with the molecular descriptions and predicted bioactivities (Tables 3 and 4). C-10 and C-11 were the only two compounds that revealed potential activity as predicted ion channel modulators with probable high activities as GPCR

Table 3 Molecular descriptors for the synthesized compounds

Compounds ID	MiLog P	TPSA (\AA^2)	MW (Da)	nON	nOHNH	NoV	nRotB	MV (\AA^3)
C-1	8.90	68.34	582.96	5	5	2	6	616.16
C-2	5.46	105.27	703.07	9	5	2	10	718.45
C-3	9.91	50.76	747.25	5	3	2	8	796.91
C-4	8.50	68.34	578.93	5	5	2	2	594.58
C-5	9.78	50.76	743.22	5	3	2	4	775.33
C-6	1.15	84.74	286.42	5	5	0	4	291.32
C-7	8.44	88.56	598.96	6	6	3	6	624.20
C-8	9.77	70.99	763.25	6	4	2	8	804.96
C-9	7.56	35.49	416.69	3	2	1	4	445.49
C-10	8.53	35.49	470.79	3	2	1	4	501.90
C-11	6.79	44.73	446.72	4	2	1	5	471.06
C-12	7.89	44.73	502.83	4	2	2	6	537.27
C-13	6.56	44.73	446.72	4	2	1	5	471.06
C-14	5.72	63.20	506.77	6	2	2	7	522.20
C-15	7.15	35.49	414.68	3	2	1	2	434.70
C-16	5.20	41.49	333.52	3	2	1	1	340.90
C-17	6.77	41.49	389.62	3	2	1	2	407.11
C-18	8.29	41.49	445.73	3	2	1	3	473.33
C-19	4.94	44.28	334.55	3	3	0	3	355.11
C-20	5.55	24.05	336.59	2	2	1	3	348.18
C-21	5.90	24.05	401.46	2	2	1	3	349.50
C-22	8.04	15.27	483.60	2	1	1	4	439.88
C-23	6.93	15.27	402.69	2	1	1	2	411.18
C-24	7.64	15.27	481.59	2	1	1	2	429.09
C-25	5.62	33.73	462.74	4	1	1	4	462.32
C-26	4.98	21.26	321.53	2	1	0	1	317.38

miLogP calculated partition coefficient, *TPSA* total polar surface area, *MW* molecular weight, *nON* number of hydrogen bond acceptors, *nOHNH* number of hydrogen bond donors, *noV* number of violations, *nrotb* number of rotatable bonds, *MV* mean molecular volume

Table 4 Predicted bioactivity potentials of the synthesized compounds

Compounds ID	GPCR ligand	ICM	KI	NRL	PI	EI
C-1	0.09	-0.36	-0.25	-0.15	0.17	-0.06
C-2	-0.52	-1.41	-1.11	-1.08	-0.21	-0.86
C-3	-1.10	-2.22	-1.84	-1.87	-0.66	-1.53
C-4	0.10	-0.34	-0.28	-0.16	0.13	-0.04
C-5	-1.10	-2.20	-1.86	-1.88	-0.69	-1.51
C-6	0.25	0.00	-0.21	-0.05	0.16	0.27
C-7	0.08	-0.45	-0.27	-0.17	0.16	-0.09
C-8	-1.25	-2.44	-2.02	-2.05	-0.79	-1.70
C-9	0.28	0.17	-0.01	0.03	0.30	0.20
C-10	0.29	0.20	-0.03	0.08	0.27	0.22
C-11	0.30	0.20	-0.02	0.05	0.37	0.23
C-12	0.28	0.15	-0.12	0.01	0.30	0.21
C-13	0.29	0.18	-0.02	0.03	0.32	0.21
C-14	0.38	0.19	0.11	0.11	0.42	0.28
C-15	0.29	0.21	-0.06	0.01	0.25	0.24
C-16	0.19	0.13	-0.18	0.28	0.19	0.31
C-17	0.16	0.01	-0.29	0.27	0.12	0.31
C-18	0.16	0.03	-0.29	0.26	0.12	0.29
C-19	0.30	0.17	-0.01	0.05	0.28	0.22
C-20	0.15	-0.04	-0.21	-0.19	0.19	0.09
C-21	0.08	-0.11	-0.28	-0.26	0.09	0.02
C-22	0.12	-0.07	-0.21	-0.24	0.14	0.03
C-23	0.29	-0.07	-0.24	-0.31	0.33	0.24
C-24	0.13	-0.04	-0.26	-0.25	0.08	0.07
C-25	0.41	0.09	-0.12	-0.15	0.47	0.35
C-26	0.16	-0.23	-0.45	-0.12	0.26	0.33

ICM ion channel modulation, KI kinase inhibition, NRL nuclear receptor ligand, PI protease inhibition, EI enzyme inhibition

ligands and enzyme inhibitors. Their selectivity could have also been enhanced by their low total polar surface area (TPSA) and moderate flexibilities (the degree of rotation of the molecules). The low anti-*T. gondii* activity of C-9 with great structural similarity to C-11, which had higher antiparasitic action and selectivity, cannot be explained yet. The moderate antiparasitic activities of C-15 to C-17 may be due to the fused phenanthrene rings (to the oxazole), which could facilitate dissociation of the heterocyclic ring, making the charged electronegative atoms (O and N) more available for membrane interactions via covalent and hydrogen bonds. Further, it appears that the presence of oxazole in C-18 greatly enhanced the selective action against the parasite when compared with the other phenyl-substituted 1*H*-imidazole compounds. In addition, the predicted nuclear receptor ligand and enzyme inhibition potentials suggest a possible mode of action of the compounds (Table 3). The low antiparasitic activity of C-19 may indicate that the stearic bulky groups shielded the imidazole ring from interacting with the parasite.

In addition, the introduction of the thiophene group (C-20 to C-22) induced a significant change in the selectivity against *T. gondii* versus the host cells. Interestingly, bromination of the thiophene at position C2 in C-21 seems to have had a significant effect, in that the host cytotoxicity increased. It may be that the introduction of bromine (Br) at position 2 of the thiophene enhanced its activity against *T. gondii* but reduced its selectivity since C-20, which lacked the bromine atom, showed lower host toxicity. Moreover, bromine is electronegative, and its presence might cause an electron-withdrawing effect, thus making the compound more reactive. Because bromine has a high electron-withdrawing potential, many brominated (or halogenated) compounds are known to be bioactive (Tessmann et al. 2017). C-23 to C-26, which had close structural similarities, also had moderate antiparasitic activities as well as similar selectivity indexes. This implies that the structural modification of the side chains had little or no effect on antiparasitic action. However, C-25 showed the highest potential to be a GPCR ligand, proteinase, and enzyme inhibitor of all the examined compounds.

It is interesting to observe that each of the five compounds (C-10, C-11, C-18, C-20, and C-21) that exhibited significant antiparasitic activity with high selectivity against the parasite versus the host cells had only one violation of Lipinski's rule of drug-likeness. Additionally, these same compounds all had positive enzyme inhibition values based on the predicted bioactivity score. These five compounds only slightly violated the partition coefficient threshold and complied with all the other rules as indicated. The other compounds, which violated other rules such as molecular weight, molecular size, total polar surface area, number of rotatable bonds, and number of hydrogen bond donors/acceptors, showed lower selective activity against *T. gondii* versus the host cells. This implies that only the partition coefficient threshold may be violated for drug candidacy to be maintained. Potential enzyme inhibition also seems to be a key factor to consider in identifying lead candidates for early drug development for *T. gondii* therapy. This discovery may guide future studies in designing drug candidates for use against *T. gondii*.

SAR and prediction of toxicological risks: molecular modeling studies

The combination of the various structural features of a compound is known to govern its bioactivity. The properties of a molecule such as hydrophobicity, electronic distribution, hydrogen bonding characteristics, molecule size, and flexibility determine the absorption (bioavailability), distribution, metabolism (reactivity), and excretion (ADME) of that molecule (Atolani et al. 2014; Rocha-Roa et al. 2018). Therefore, applying the online cheminformatics tool, Molinspiration, afforded the determination of the properties related to following Lipinski's rule of five, according to which the optimum

properties are the partition coefficient ($\text{miLog}P$) of < 5.0 , molecular weight ≤ 500 , hydrogen bond acceptors 10, and donors 5. The rule was further expanded to include the number of rotatable bonds (ten or fewer) and a total polar surface area (TPSA) equal to or less than 140 \AA^2 as ideal parameters for drug-likeness. Furthermore, compounds violating more than one rule demonstrate a reduced oral bioavailability potential (Flores-Holguín and Glossman-Mitnik 2004). The result of molecular modeling studies (Tables 3 and 4) provided additional insights into the physicochemical features of the compounds and buttressed the SAR in explaining the in vitro anti-*T. gondii* studies.

Following Lipinski's rules, of the class A series, the bis-imidazoles, only compound C-6 with the smallest molecular size and volume did not violate more than one rule (Table 3). This may account for the generally low bioactivity score for the class (Table 4). Of particular interest is compound C-7, which had three violations (partition coefficient, molecular weight, and number of hydrogen bond donors). This finding correlates with an extremely low bioactivity score for C-7 (Table 3). In classes B and C, series C-9 to C-23, only

compounds C-12 and C-14 with a relatively high $\text{miLog}P$ (> 5) and molecular weight (> 500 Da) violated two Lipinski's rules, while the others violated either one or none. Compounds C-6, C-9, C-10, C-11, C-12, C-13, C-14, C-15, C-19, C-23, and C-25 showed high potentials as GPCR ligands, while of the entire series only C-10 and C-11 had a significant predicted ion channel modulation potential (Table 4). However, only C-16, C-17, and C-18 showed good bioactivity scores as nuclear receptor compounds and high scores as enzyme inhibitors. This could be the result of the phenanthro[9,10-d] moiety, which was uniquely present in their structures. C-14 and C-25 exhibited the highest potential protease inhibition scores of 0.42 and 0.47, respectively. C-25 showed the highest potential on the basis of having GPCR ligand and enzyme inhibitor scores of 0.41 and 0.35, respectively.

In addition, the imidazole compounds were ranked based on toxicological risks prediction using PROTOX II modeling. The oral toxicity prediction results showed that majority of the compounds belong to classes 3, 4, and 5 except C-26 which is class 6 (Table 5). The prediction accuracy ranged between

Table 5 Sorting of imidazole compounds based on possible toxicological risks using PROTOX II

Compound IDs	Toxicity class	LD ₅₀ ^a (mg/kg)	Average similarity	Prediction accuracy
C-1	3	300	70.09	69.26
C-2	4	1190	100	100
C-3	4	2000	62.09	67.38
C-4	5	5000	61.18	68.07
C-5	4	1000	60.58	68.07
C-6	4	1000	44.76	54.26
C-7	4	2000	68.47	68.07
C-8	4	2000	52.07	67.38
C-9	4	2000	52.80	67.38
C-10	4	2000	52.46	67.38
C-11	4	2000	53.54	67.38
C-12	4	2000	53.76	67.38
C-13	4	2000	55.58	67.38
C-14	4	2000	50.66	67.38
C-15	4	595	61.77	68.07
C-16	4	1600	76.53	69.26
C-17	4	1600	74.23	69.26
C-18	4	1600	72.32	69.26
C-19	3	300	76.15	69.26
C-20	3	300	54.57	67.38
C-21	3	300	50.06	67.38
C-22	4	2000	40.46	52.26
C-23	4	770	50.45	67.38
C-24	4	1000	46.37	54.26
C-25	5	3420	48.26	54.26
C-26	6	10,000	79.22	69.26

^a Oral toxicity

Table 6 Probability for toxicity endpoints by modeling on PROTOX II

Compound IDs	HPT ^a	CCG ^a	IMMT ^a	MUTG ^a	CYTOX ^a	AhR ^a	MMP ^a	ART ^a	PP ₅₃ ^a
C-1	–	–	–	0.72	–	–	–	–	–
C-2	–	–	–	0.75	–	–	–	–	–
C-3	0.54	0.52	–	0.50	–	0.51	–	–	–
C-4	0.55	–	–	0.72	–	0.61	–	–	–
C-5	0.53	0.52	–	–	–	–	–	–	–
C-6	–	–	–	–	–	–	–	–	–
C-7	0.54	–	–	0.69	–	–	–	–	–
C-8	0.54	–	–	–	–	–	–	–	–
C-9	0.56	0.53	–	–	–	–	–	–	–
C-10	–	–	–	–	–	–	–	–	–
C-11	0.51	0.54	0.53	0.55	–	–	–	–	–
C-12	–	–	0.71	–	–	–	–	–	–
C-13	0.51	0.54	–	0.55	–	–	–	–	–
C-14	–	0.51	0.52	0.50	0.59	–	–	–	–
C-15	0.54	0.52	–	0.61	0.58	–	–	–	–
C-16	0.55	0.54	0.55	–	0.53	–	–	–	–
C-17	–	–	0.70	–	–	–	0.53	–	–
C-18	–	–	0.90	–	–	–	0.53	–	–
C-19	0.55	–	–	0.77	–	–	–	–	–
C-20	0.56	–	–	0.76	–	–	–	–	0.52
C-21	0.60	–	–	0.60	–	0.51	–	–	–
C-22	0.56	–	–	–	–	0.51	–	0.60	–
C-23	0.52	–	–	0.68	–	0.61	–	–	–
C-24	0.55	–	–	0.59	–	0.53	–	0.53	–
C-25	–	–	–	0.65	0.52	0.52	–	–	–
C-26	0.61	0.50	–	–	–	–	–	–	–

– means no detectable binding

HPT hepatotoxicity, *CCG* carcinogenicity, *IMMT* immunotoxicity, *MUTG* mutagenicity, *CYTOX* cytotoxicity, *AhR* aryl hydrocarbon receptor, *MMP* mitochondrial membrane potential, *ART* aromatase, *PP₅₃* phosphoprotein (tumor suppressor) p53

^aProbability

52.26 and 100%, while the average similarity lies between 40.46 and 100%. For the toxicity endpoint modeling, the prediction results showed that 65.39% (17) of the imidazole compounds may be potentially hepatotoxic, while 34.62% (9) have carcinogenic tendency (Table 6). Also, of the 26 compounds,

6 (23.08%), 15 (57.69%), 4 (15.38%), 7 (26.92%), 2 (7.69%), 2 (7.69%) and 1 (3.85%) respectively were found to be immunotoxic, mutagenic, cytotoxic, and modulator of AhR, aromatase, MMP, and phosphoprotein P53. Meantime only C-19 and C-26 showed binding to toxicity targets. C-19 binds

Table 7 Toxicity target binding prediction using PROTOX II

Compound IDs	Toxicity target	Average pharmacophore fit (%)	Average ligand similarity (%)
C-10	Prostaglandin G/H synthase I	0.00	80.44
C-11	Prostaglandin G/H synthase I	0.00	75.1
C-12	Prostaglandin G/H synthase I	0.00	75.52
C-13	Prostaglandin G/H synthase I	0.00	78.95
C-14	Prostaglandin G/H synthase I	0.00	72.41
C-19	Amine oxidase	26.84	0.00
C-26	Prostaglandin G/H synthase I	31.94	0.00

amine oxidase with average pharmacophore fit of 26.84%, while C-26 binds prostaglandin G/H synthase I (PGH1) with a fit of 31.94% (Table 7). Both C-19 and C-26 had 0.00% average ligand similarity in this regard. Additionally, C-10, C-11, C-12, C-13, and C-14 had average ligand similarity between 72.41 and 80.44% for PGH1 target binding.

Conclusion

We report the synthesis and biological potentials of imidazole derivatives, a new class of potential anti-*T. gondii* compounds. The substituents and their location impacted the bioactivity and physicochemical properties. The combination of the structural features reported for the compounds is believed to govern the anti-*T. gondii* activities of the compounds studied. We also confirmed that a small structural modification, as in the oxazole derivative of C-16 to yield C-18, could lead to unexpected bioactivity and selectivity. The data herein depict promising evidence warranting further exploration of imidazole derivatives, especially compounds C-10, C-11, C-12, C-14, C-16, C-18, C-20, and C-21 with high selective activities towards the parasite versus host cell, as possible source of alternative and effective anti-*T. gondii* agents. Further investigations to determine the anti-*T. gondii* potential of imidazole derivatives in a mouse model as well as the mode of antiparasitic action with the goal of developing new and effective treatment strategies for acute and/or latent toxoplasmosis form part of our future research efforts.

Acknowledgments The authors would like to thank the Department for Management of Science and Technology Development, Faculty of Applied Science, Ton Duc Thang University, Ho Chi Minh City. The JSPS Fellowship to OS Adeyemi is also acknowledged. Also, AO Eseola appreciates the Alexander von Humboldt Foundation support through the Georg Forster postdoctoral scholarship and the Redeemer's University for fellowship leave. Additionally, the financial support by the Deutsche Forschungsgemeinschaft (DFG) is appreciated (PL 155/11, PL 155/12, and PL155/13). For editorial assistance, our appreciation goes to Ed and Rhoda Perozzi and Carey Johnson of the Chemistry Department, University of Kansas, USA.

Compliance with ethical standards

Conflict of interest The authors declare that they have no competing interest.

References

- Adeyemi OS, Molina MT, Eseola AO, Fonseca-Berzal C, Gómez-Barrio A (2017a) New imidazole compounds active against *Trypanosoma cruzi*. *Comb Chem High Throughput Screen* 20:20–24
- Adeyemi OS, Murata Y, Sugi T, Kato K (2017b) Inorganic nanoparticles kill *Toxoplasma gondii* via changes in redox status and mitochondrial membrane potential. *Int J Nanomed* 12:1647–1661
- Adeyemi OS, Murata Y, Sugi T, Han Y, Kato K (2017c) Modulation of host HIF-1 α activity and the tryptophan pathway contributes to the anti-*Toxoplasma gondii* potential of nanoparticles. *Biochem Biophys Res* 11:84–92
- Adeyemi OS, Sugi T, Han Y, Kato K (2018a) Screening of chemical compound libraries identified new anti-*Toxoplasma gondii* agents. *Parasitol Res* 117:355–363
- Adeyemi OS, Murata Y, Sugi T, Han Y, Kato K (2018b) Exploring amino acid-capped nanoparticles for selective anti-parasitic action and improved host biocompatibility. *J Biomed Nanotechnol* 14:847–867
- Adeyemi OS, Molefe NI, Awakan OJ, Nwonuma CO, Alejelowo O, Olaolu T, Maimako RF, Suganuma K, Han Y, Kato K (2018c) Metal nanoparticles show potential to restrict *Trypanosoma* growth. *Artif Cells Nanomed Biotechnol* 46:S86–S94
- Adeyemi OS, Otohinoi DA, Awakan OJ, Adeyanju AA (2019) Cellular apoptosis of HFF cells by inorganic nanoparticles not susceptible to modulation by *Toxoplasma gondii* infection *in vitro*. *Toxicol in Vitro* 54:280–285
- Alday PH, Doggett JS (2017) Drugs in development for toxoplasmosis: advances, challenges, and current status. *Drug Des Dev Ther* 11: 273–293. <https://doi.org/10.2147/DDDT.S60973>
- Atolani O, Fabiya OA, Olatunji GA (2014) Isovitexin from *Kigelia pinnata*, a potential eco-friendly nematicidal agent. *Trop Agric* 91: 67–74
- Berkelhammer G, Asato G (1969) 2-Amino-5-(1-methyl-5-nitro-2-imidazolyl)-1,3,4-thiadiazole: a new antimicrobial agent. *Science* 162:1146–1148
- Castro JA, de Mecca MM, Bartel LC (2006) Toxic side effects of drugs used to treat Chagas' disease (American trypanosomiasis). *Hum Exp Toxicol* 25:471–479
- Coura JR, Castro SL (2002) A critical review on Chagas disease chemotherapy. *Mem Inst Oswaldo Cruz* 97:3–24
- Dzitko K, Paneth A, Plech T, Pawelczyk J, Węglińska L, Paneth P (2014 Dec) Triazole-based compound as a candidate to develop novel medicines to treat toxoplasmosis. *Antimicrob Agents Chemother* 58(12):7583–7585. <https://doi.org/10.1128/AAC.03832-14>
- Eseola AO, Li W, Sun WH, Zhang M, Xiao L, Woods JAO (2011) Luminescent properties of some imidazole and oxazole based heterocycles: syntheses, structures, substituent and solvent effects. *Dyes Pigm* 88:262–273
- Eseola AO, Adepitan O, Görls H, Plass W (2012) Electronic/substituents influence on imidazole ring donor-acceptor capacities using 1*H*-imidazo [4,5-*f*][1,10]phenanthroline frameworks. *New J Chem* 36: 891–902
- Eseola AO, Görls H, Bangesh M, Plass W (2018) ES IPT-capable 2,6-di(1*H*-imidazol-2-yl)phenols with very strong fluorescent sensing signals towards Cr(III), Zn(II) and Cd(II): molecular variation effects on turn-on efficiency. *New J Chem* 42:7884–7900
- Eseola AO, Görls H, Plass W (2019) Importance of monodentate monoligand designs in developing N-stabilized Pd catalysts for efficient ambient temperature C C coupling: donor strengths and steric features. *Mol Catal* 473:110398. <https://doi.org/10.1016/j.mcat.2019.110398>
- Finlayson K, Witchel HJ, McCulloch J, Sharkey J (2004) Acquired QT interval prolongation and HERG: implications for drug discovery and development. *Eur J Pharmacol* 500:129–142
- Flegler J, Prandota J, Soviejkova M, Israili ZH (2014) Toxoplasmosis—a global threat. Correlation of latent toxoplasmosis with specific disease burden in a set of 88 countries. *PLoS ONE* 9:e90203
- Flores-Holguín N, Glossman-Mitnik D (2004) CHIH-DFT determination of the molecular structure, infrared and ultraviolet spectra of the antiparasitic drug megalol. *J Mol Struct* 681:77–82
- Flores-Holguín N, Glossman-Mitnik D (2005) CHIH-DFT determination of the reactivity sites of the antiparasitic drug megalol. *J Mol Struct* 723:231–234

- Fonseca-Berzal C, Ruiz FAR, Escario JA, Kouznetsov VV, Gomez-Barrio A (2014) *In vitro* phenotypic screening of 7-chloro-4-amino(oxy) quinoline derivatives as putative anti-*Trypanosoma cruzi* agents. *Bioorg Med Chem Lett* 24:1209–1213
- Grellier P, Sinou V, Garreau-de Loubresse N, Bylen E, Boulard Y, Schrevel J (1999) Selective and reversible effects of vinca alkaloids on *Trypanosoma cruzi* epimastigote forms: blockage of cytokinesis without inhibition of the organelle duplication. *Cell Motil Cytoskeleton* 42:36–47
- Harrell M, Carvounis PE (2014) Current treatment of toxoplasma retinochoroiditis: an evidence-based review. *J Ophthalmol* 273506. <https://doi.org/10.1155/2014/273506>
- Kamau ET, Srinivasan AR, Brown MJ, Fair MG, Caraher EJ, Boyle JP (2012) A focused small-molecule screen identifies 14 compounds with distinct effects on *Toxoplasma gondii*. *Antimicrob Agents Chemother* 56:5581–5590
- Lavorato SN, Duarte MC, Lage DP, Tavares CAP, Coelho EAF, Alves RJ (2017) Synthesis and antileishmanial activity of 1,3-bis(aryloxy)propan-2-amines. *Med Chem Res* 26:1052–1072
- Liesen AP, de Aquino TM, Carvalho CS, Lima VT, de Araujo JM, de Lima JG, de Faria AR, de Melo EJT, Alves AJ, Alves EW (2010) Synthesis and evaluation of anti-*Toxoplasma gondii* and antimicrobial activities of thiosemicarbazides, 4-thiazolidinones and 1,3,4-thiadiazoles. *Eur J Med Chem* 45:3685–3691
- Lipinski CA (2004) Lead- and drug-like compounds: the rule-of-five revolution. *Drug Discov Today Technol* 1:337–341
- Lipinski CA, Lombardo F, Dominy BW, Feeney PJ (1997) Experimental and computational approaches to estimate solubility and permeability in drug discovery and development settings. *Adv Drug Deliv Rev* 23:4–25
- Lipinski CA, Lombardo F, Dominy BW, Feeney PJ (2001) Experimental and computational approaches to estimate solubility and permeability in drug discovery and development settings. *Adv Drug Deliv Rev* 46:3–26
- Qasim M, Abideen Z, Adnan MY, Gulzar S, Gul B, Rasheed M, Khan MA (2017) Antioxidant properties, phenolic composition, bioactive compounds and nutritive value of medicinal halophytes commonly used as herbal teas. *S Afr J Bot* 110:240–250
- Rocha-Roa C, Molina D, Cardona N (2018) A perspective on thiazolidinone scaffold development as a new therapeutic strategy for toxoplasmosis. *Front Cell Infect Microbiol* 8:360. <https://doi.org/10.3389/fcimb.2018.00360>
- Rutkowska E, Pajak K, Józwiak K (2017) Lipophilicity—methods of determination and its role in medicinal chemistry. *Acta Pol Pharm* 70:3–18
- Tessmann JW, Buss J, Begnini KR, Berneira LB, Paula FR, de Pereira CMP, Collares T, Seixas FK (2017) Antitumor potential of 1-thiocarbamoyl-3,5-diaryl-4,5-dihydro-1-Hpyrazoles in human bladder cancer cells. *Biomed Pharmacother* 94:37–46

Supplementary material CCDC 850686, 1897702, and 1897701 contain the supplementary crystallographic data for compounds **C-7**, **C-10**, and **C-25**, respectively. These data can be obtained free of charge on application to CCDC, 12 Union Road, Cambridge CB2 1EZ, UK (fax: +44 01223 336033; e-mail: deposit@ccdc.cam.ac.uk).

Publisher's note Springer Nature remains neutral with regard to jurisdictional claims in published maps and institutional affiliations.